

SoLID pre-R&D

Quarterly Progress Report

August 2021 to January 2022

SoLID Collaboration

January 10, 2025

Contents

1 Project Summary	3
2 DAQ	3
2.1 Q6 activities	3
2.2 Summary of activities	3
2.3 Detailed reports	6
2.3.1 GEM testing	6
2.3.2 DAQ test stand and rate tests	9
2.4 Summary of activities of the project	12
2.4.1 A : GEM VMM readout	12
2.4.2 B : APV fast readout	13
2.4.3 C : Flash ADC based trigger and fast FADC VXS readout	13
2.4.4 D : Gas Cerenkov	14
2.4.5 E : Time of flight	14
2.5 Budget / spending summary / procurement	14
3 High Rate Test of MaPMT Array and LAPPD Using a Telescopic Cherenkov Device	16
3.1 Summary	16
3.1.1 Quarterly Summary	16
3.1.2 Project Summary	16
3.2 Project Milestones	18
3.3 Budget and expense summary	18
3.4 Analysis and Simulation	19
3.5 MaPMT with MAROC sum readout bench test	21

3.5.1	Sum saturation study	21
3.5.2	Pixel TDC threshold study	22
3.5.3	LED Ring analysis	24
3.5.4	Cosmic test	26
3.6	Discrepancies between measured and simulated NPE count and possible sources of NPE inefficiency	29

1 Project Summary

This is the final quarterly report submitted to DOE, signifying the end of the project term. Broadly, this project has been successful in completing the proposed objectives. We verified the proposed design presented in the SoLID pre-CDR for the Cherenkov detectors and the DAQ readout electronics system. We tested the performance of the Cherenkov detectors and DAQ system with a real electron beam condition and/or bench setup using radioactive source at or beyond the high rates expected for the approved SoLID experiments. All four milestones for the Cherenkov testing part have been met. For the DAQ part, thirteen of the fifteen milestones have been met. For the two milestones related to VMM readout system, there are some delays and they are expected to be reached in May with a separate summary to be submitted as a supplement at that time. Detailed summaries of the milestones and goals of both the DAQ and Cherenkov pre-R&D activities are presented in their respective sections below.

2 DAQ

2.1 Q6 activities

In the last quarter, developments of the FADC readout and triggering, testing of readout for the Cherenkov and the Time of flight were completed. The final testing of the VMM readout in high background is awaiting the manufacturing and delivery of the final prototype which was delayed to late April 2022.

2.2 Summary of activities

This chapter summarizes the SoLID DAQ pre-R&D activities for the sixth quarter, August, 2021 to March, 2022.

The five main tasks (A-E) are:

- A) GEM VMM3 readout high rate testing to determine trigger rate capability, behavior with pile-up, and readout performance

Milestone	Objectives	Expected Completion Date	Status	Updated Date
A1	Finish development of VMM3 direct readout	May 1, 2020	Complete Q2	
A2	High rate testing with detector	August 1st 2021	90% complete	May 2022
A3	Optimized VMM3 setup for maximum data rate	July 1st,2021	90% complete	May 2022

Instead of a modified version of the evaluation board, a new high performance VMM prototype was designed to be close to what will be used for the actual experiment. The board had to go through several design iterations to address a few technical issues and will be fabricated in April and tested in May. We plan to have a separate write-up as a supplement to the final quarterly report to summarize and conclude this activity.

The test with detector using X-ray source could not be completed with the evaluation board, since we found that only 12 channels out of 128 were connected to the direct output. The final test will be done with the final prototype board, allowing it to instrument 2x256 strip of a small GEM chamber.

- B) GEM APV25 readout high rate testing: show that 100 kHz trigger rate is achievable with existing readout hardware developed for SuperBigBite (SBS).

Milestone	Objectives	Expected Completion Date	Status
B1	Finish development of fast APV25 readout	November 1, 2020	Complete Q2
B2	Determine maximum rate achievable with APV25	March 15, 2021	Complete Q3

- C) FADC developments for fast readout and triggering

Milestone	Objectives	Expected Completion Date	Status
C1	Development of FADC readout through VXS	November 1, 2020	Complete Q4
C2	Testing PVDIS trigger functionalities and rate capability	August 1, 2021	Complete Q5
C3	PVDIS trigger test with two sectors	July 15, 2021	Complete Q6
C4	Test SIDIS trigger	August 15, 2021	Complete Q6

C3 and C4 were completed in the last quarter. The dead-time of the system was measured up to 120 KHz with a loss of around 1% at 120 KHz, satisfying the SIDIS requirements and less than 0.2% at 30 KHz, satisfying the PVDIS requirements.

- D) Test of gas Cherenkov readout with analog sums and MAROC chip

Milestone	Objectives	Expected Completion Date	Status
D1	Setup FADC crate for Cherenkov simple sum testing	February 15, 2020	Complete Q1
D2	Record beam data using simple sum and FADC	September 15, 2020	Complete Q3
D3	Record data using MAROC sum readout	Oct 15, 2020	Complete Q6

This item is complete. More details are given in the Cherenkov section

- E) Time of flight using the NALU sampling chip

Milestone	Objectives	Expected Completion Date	Status
E1	Acquire and setup ASOC evaluation board	April 15, 2020	Complete Q3
E2	Acquire data of scintillator	October 15, 2020	Complete Q4
E3	Complete analysis and determine achieved timing resolution with ASOC and compare to FADC resolution	August 15, 2021	Complete Q6

Data were taken with cosmic rays and with a radioactive source. The intrinsic timing resolution is around 20 ps, which is better than what can be achieved using the FADC alone, where only a timing resolution of 150 ps can be reached. Pile-up as close as 4 ns apart could be separated. The dynamic range of the SPD is a bit on the low side, but the final detector will have a built-in amplifier to better use the dynamic range of the chip. Some developments will be required to integrate the system in the DAQ system for testing with all the detectors and to evaluate the dead time performance of the system in beam conditions.

2.3 Detailed reports

2.3.1 GEM testing

A) VMM3 We are studying the behavior of the VMM3 with high background and are determining the maximum trigger rate that can be achieved.

A3: Prototype front-end board – The mezzanine boards for power and communication were completed and manufactured. Overall project timeline has delayed by about 7 months, mainly due to several revisions to improve the design and fix minor technical issues:

- VMM chip testing issues (2 months)
- design revision to accommodate UVA GEM geometry (1 month)
- design change board-to-board connector types to ensure mating tolerance can be met (1 month)
- design change power delivery system to enable current monitoring for critical voltage rails of FPGA (1 month)



Figure 1: VMM prototype board (top) with dual power mezzanine cards

- design change driver translation circuit from FPGA to VMM (SLVS). Required simulation. (1 month)
- new detector setup for radioactive source testing (3 months)
- PCB layout improvements for VMM after review by De Geronimo (1 month)

A2: Final test will use the prototype board with the X-ray setup at UVA to evaluate the performance of the chip in a high background environment.

A small GEM detector has been setup and tested with the existing VMM boards while we are waiting for the final prototype using radioactive source and cosmic rays. By using a Fe⁵⁵ source the signal of the VMM was recorded with different shaping times available.

The amplitude for 25 ns shaping is only lower by about 20%, which can be compensated by available gain. This shows the GEM signal is quite fast with main part in first 25 ns and whole pulse shorter than 100 ns.

Data taken with cosmic rays using the neighboring strip logic show that the signal is well separated from the pedestal.

The VMM dynamic range is well matched with the charge produced in the GEM. The level of noise is sufficiently low so that the current version of VMM is usable for SoLID as is.

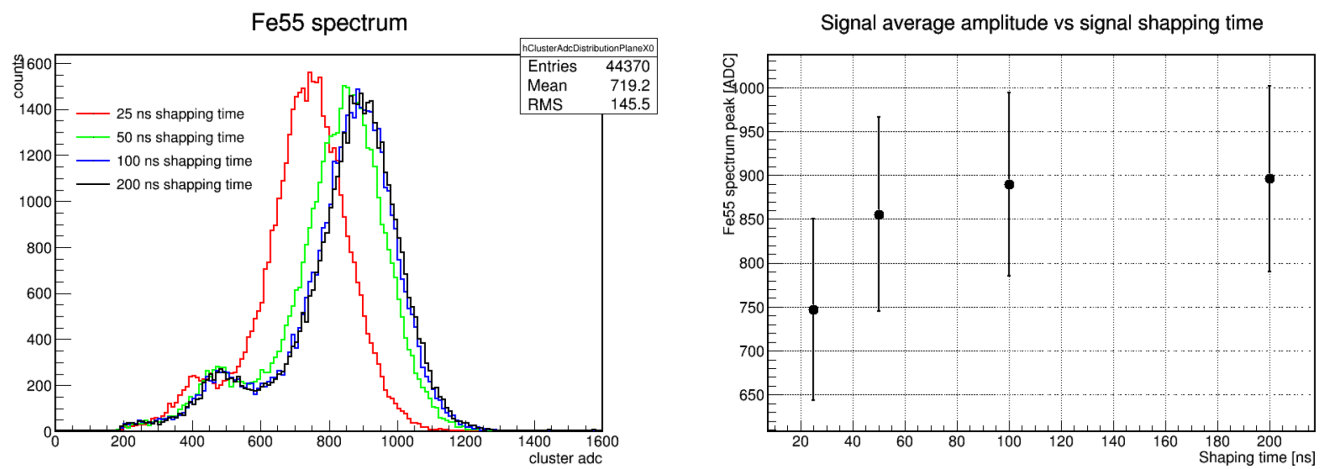


Figure 2: Fe^{55} signal for different VMM shaping times

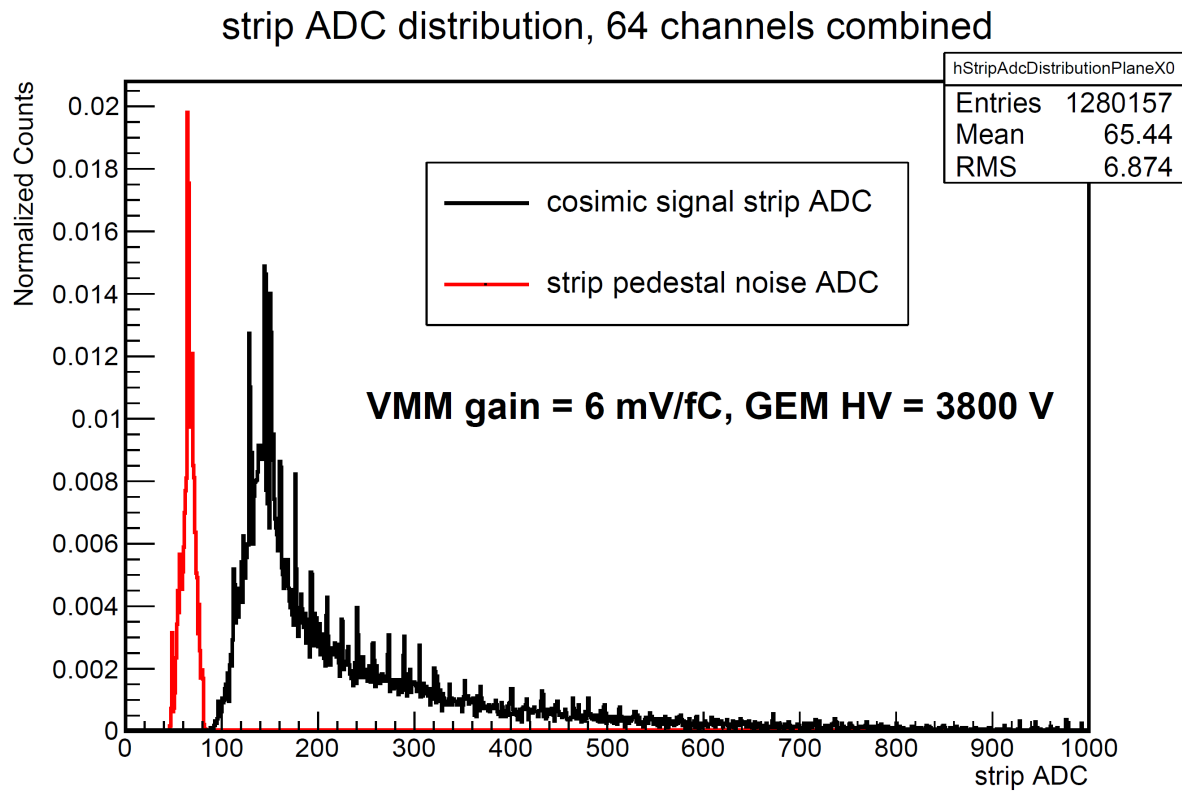


Figure 3: VMM cosmics signal

2.3.2 DAQ test stand and rate tests

C1 The Fast readout was completed in previous quarter. Data rates up to 900 MB/s could be reached about 4 times improvement compared to VME readout.

FADC fast readout firmware developed by the DAQ experts at Jefferson Laboratory, has been applied to the UMass test stand. It allows the FADC data to be read out through the VTP instead of the VME CPU. The layout of the test stand is shown in Figure 4.

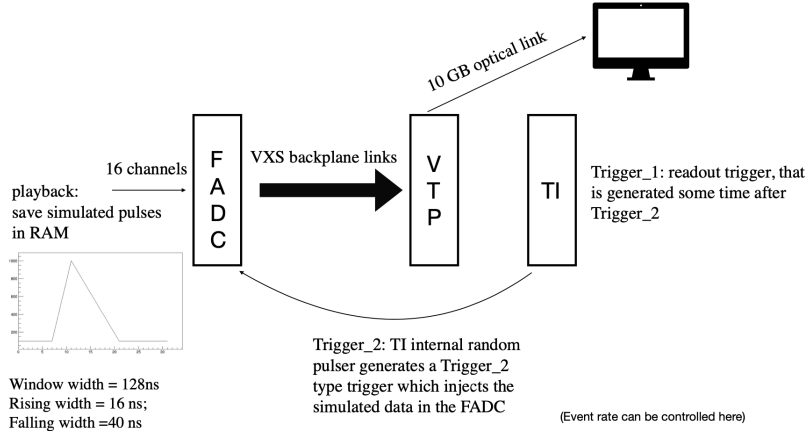


Figure 4: Layout of the FADC fast readout test

The FADC readout data are sent to the VTP over the VXS backplane links and transported through a 10 Gps optical link to the disk. The random pulser inside of the TI is used to generate the readout triggers and load the simulated pulses into the FADC. The trigger rate changed from 2 kHz to 120 kHz, and 16 FADC channels were read out with a window of 128 ns. The dead time of the DAQ with the fast readout applied is shown in Figure 5. Compared with the dead time of using VME readout, a huge improvement is observed.

C2: Calorimeter trigger Completed in quarter 5

C3 : PVDIS trigger test with two crates In SOLID experiments, the event trigger will be generated using data from multiple DAQ crates. For example, there will be more than 1700 FADC channels of the electron Calorimeter, while one VXS crate can only hold 256 FADC channels. The data transferring between VXS crates through VTP are required to form triggers.

The data transferring between two VXS crates are tested by assuming that each crate holds the FADC channels from one sector of the Calorimeter. The data from the blocks at the edge of a sector need to be transferred to the neighboring sector for the cluster identification. The potential clusters at the edges are marked in Figure 6 in orange. Because the sector is not symmetric, the left edge and the right edge need to be treated differently. The half blocks

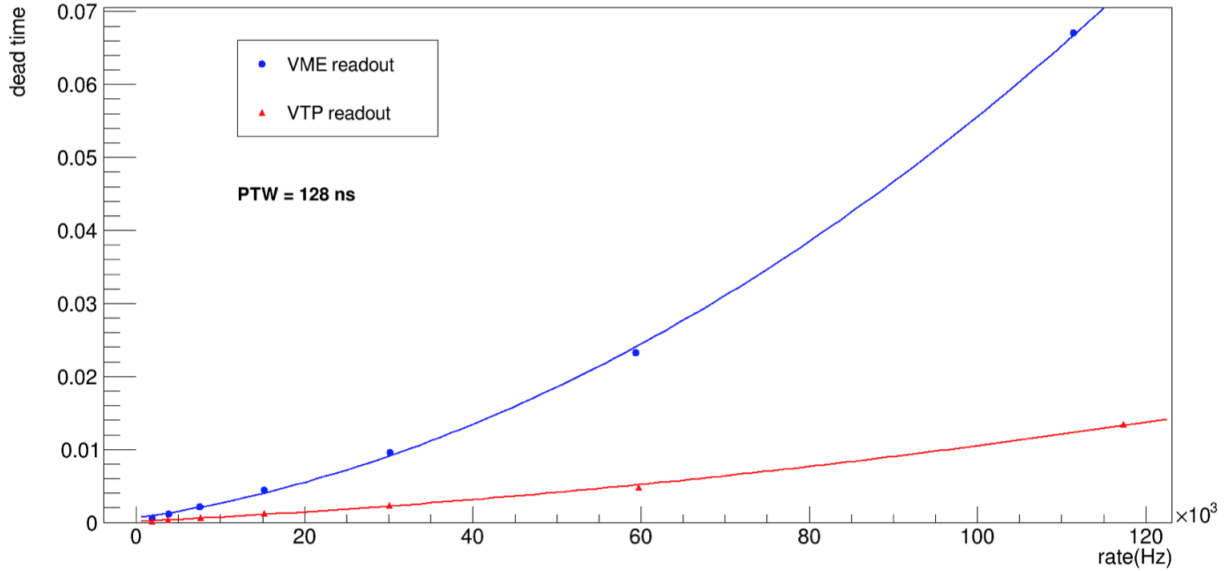


Figure 5: DAQ dead time with fast readout applied, compared with that with VME readout

at the right edge make things complicated, so it is not considered in this test. Only the left side blocks are considered in the testing. The layout of the test is shown in Figure 7. The data from the 14 FADC channels, which read out the non-half-block edge of the left sector, were transferred by the VTP to the central sector's VTP through a 32-channel optical fiber. Three simulated clusters are loaded into the FADCs to test the data transferring and the cluster finding algorithm. The reported cluster information from the central sector's VTP agree with the real clusters, shown in Figure 8. Both the data transferring from one VTP to the other VTP, and the cluster finding algorithm worked well.

A note for the Calorimeter design: if the sectors are symmetric, it would make the trigger algorithm design much easier.

C4 : SIDIS trigger test SIDIS trigger logic was implemented for the Cerenkov beam test. Different triggers including a coincidence between the calorimeter trigger, two planes of scintillator and the cerenkov all fed into the FADCs were implemented. Minimum coincidence width is 4 ns with steps of 4 ns. The coincidence window is only limited by the timing jitter of the detectors. The system was tested in Q6 with pulsers up to 120 KHz. As shown in previous section deadtime at 120 kHz was around 1%.

D) Cherenkov readout D3: The MAROC sum electronics were delivered from INFN and ready to move into Hall C. However, due to a lack of available beam time, the beam test of the MAROC sum electronics was cancelled. We then started its bench testing using lasers, LEDs, and cosmic rays. We finished the laser and LED test in the previous quarters and the cosmic ray test was finished this quarter. More details are in the Cherenkov section 3.5.

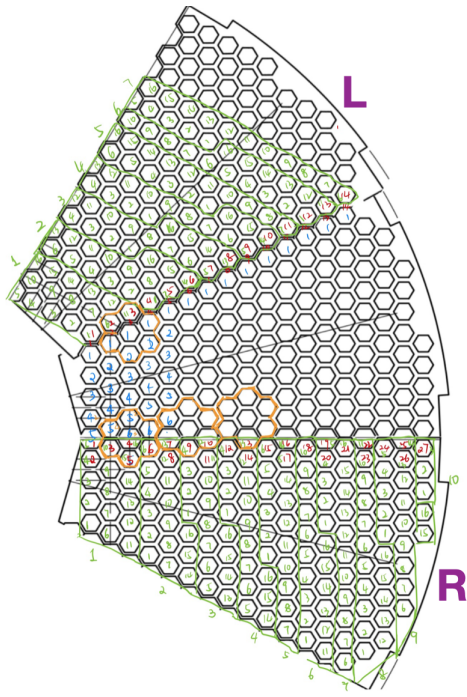


Figure 6: Clusters (Orange) at the share edge between two sectors.

E) Time of flight The current baseline readout of the TOF is based on the FADC250 with at 250 MHz sampling rate with a target goal of 100 ps timing resolution. The ASOC chip has a sampling rate from 2.4 to 3.2 GHz. We are evaluating the benefit of higher sampling rate on timing resolution in a high background environment.

- E1: Completed in the first quarter.
- E2: Complete cosmics data was taken with scintillator with custom NALU software. Figure 9 shows a signal from cosmics in the scintillator.

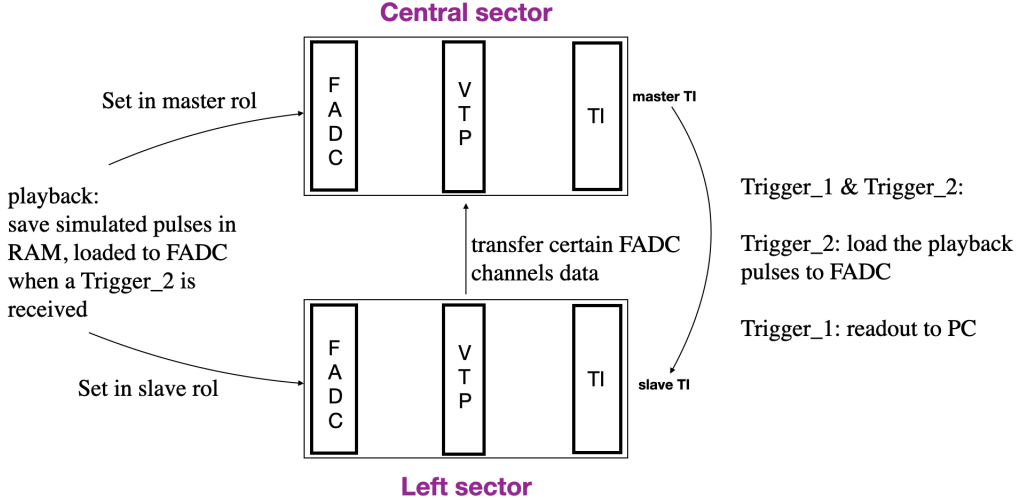


Figure 7: The layout of two crate communication testing

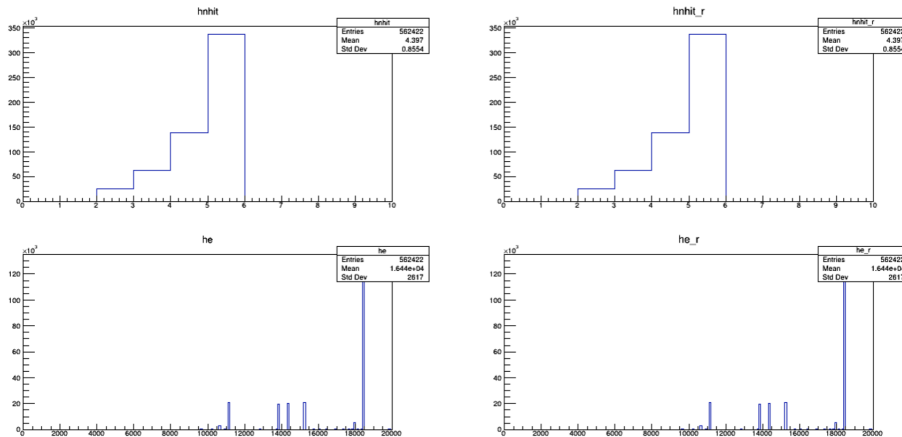


Figure 8: Left: VTP reported number of blocks triggered in a cluster and energy of a cluster; Right: real number of blocks triggered in a cluster and real energy of a cluster calculated using FADC data.

2.4 Summary of activities of the project

2.4.1 A : GEM VMM readout

Testing of the VMM board shows promising results. One critical point was the demonstration of the ability to operate a GEM chamber using the 25 ns shaping time. The amplitude of the signal is reasonably in the VMM dynamic range. Thus the current version of VMM3 can be used. A VMM based prototype board was designed and being produced. It will allow us to evaluate the performance of the system with a design close to the final design that will be used for SoLID.

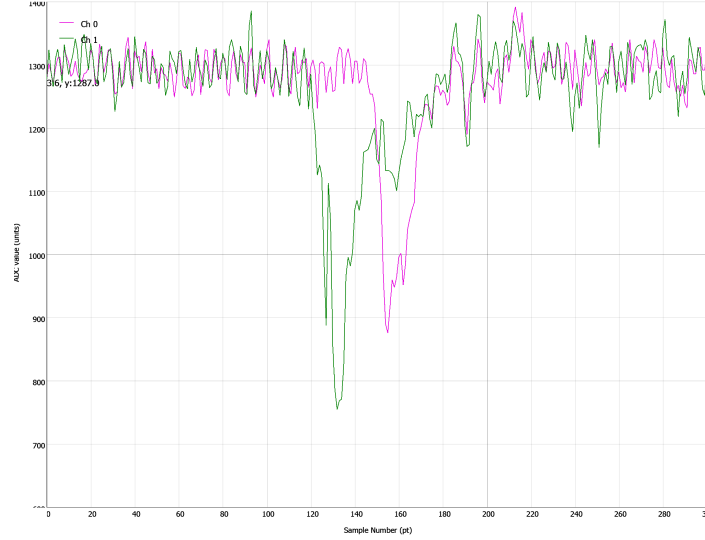


Figure 9: Example of cosmics pulse with scintillator recorded with ASOC

2.4.2 B : APV fast readout

The optical readout of MPD system was implemented using both VME backplane (up to 100 MB/s) and VXS backplane (up to 900 MB/s). The optical readout satisfies the SIDIS requirements. A flaw in the existing MPD design was discovered that would limit maximum trigger rate to 100 KHz with one sample and 30% occupancy and 12 APV per MPDs. If the MPDs are replaced, the data rate capability could be doubled at an additional cost. The system was successfully tested in beam during the SBS experiment.

2.4.3 C : Flash ADC based trigger and fast FADC VXS readout

The VXS readout was implemented for the FADC. In this scheme the transfer rate per board increases to 1.2 GB/s and each board can be read in parallel effectively increasing the bandwidth by about 160.

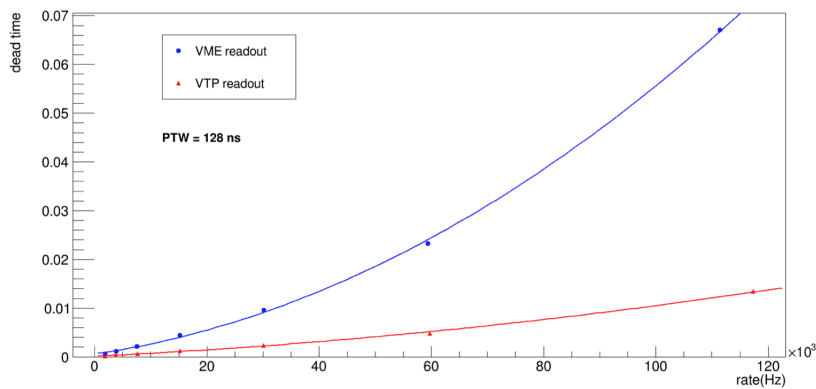


Figure 10: DAQ dead time with fast readout applied, compared with that with VME readout

The measured deadtime was of the order of 0.2% at 100% occupancy for 128 ns window which should be adequate for PVDIS. Readout up to 120 KHz was tested with a dead-time up to 1% level. With this level of performance, full waveform readout is technically possible for SIDIS but this would require a way to efficiently reduce the large amount of data to be recorded on tape.

2.4.4 D : Gas Cerenkov

The beam test was successfully recorded using FADC and digital trigger based on FADC. A modified board based on the CLAS12 design allowing the output of analog sum of the pixels was also produced and tested. See the next section about the Gas Cerenkov for the results.

2.4.5 E : Time of flight

Evaluation boards were procured and tested with both pulsers and detector. Intrinsic time resolution of the electronics is better than 20 ps which is sufficient for the high resolution time of flight.

2.5 Budget / spending summary / procurement

System	Cost (\$)	Number	Total	Spent
VXS crate for DAQ modules	15,000	2	30,000	32,388
VTP - Module for triggering and data movement	10,000	2	20,000	17,050
SSP	6,500	1	6,500	0
TI - Trigger Interface	3,000	2	6,000	0
SD - Signal Distribution card	2,500	2	5,000	1,250
FADC trigger distribution card	2,000	2	4,000	4000
VME CPU	4,500	2	9,000	11,000
Trigger Supervisor	3,500	1	3,500	0
Hardware components for VMM readout test stand	25,000	1	25,000	39,400
APV25 GEM system	23,000	1	23,000	24,000
Cables/patch	400	160	64,000	47,200
Optical fibers	100	20	2,000	2,000
MAROC eval board	23,000	1	23,000	0
ASOC eval board	10,000	1	10,000	8000
Optical transceivers	50	32	1600	1600
Total M/S direct			232,600	187,888
Total request M/S			245,928	196,654
Workforce 2020	\$130,000	1.25	162,500	90,000
Workforce 2021	\$133,900	1	133,900	203,518
Contract DG electronics	78,250	1	78,250	78,250

Table 1: Budget summary

Main expenses were for the VMM prototype board which is also ending up more expensive to meet the deadline because of the FPGA shortage this year. Cables for PVDIS calorimeter trigger tests were ordered. A modified MPD board was designed to increase the maximum data rate of APV readout by a factor of 2 and was ordered. The remaining amount of money will be spent on production of the VMM prototype boards.

	Budget (\$)	Obligated (\$)
Material	245,928	196,654
Personel	354,072	354,072
Total	600,000	550,726

Table 2: Budgeted and obligated funds summary (includes overhead)

3 High Rate Test of MaPMT Array and LAPPD Using a Telescopic Cherenkov Device

3.1 Summary

3.1.1 Quarterly Summary

This final quarterly report describes light-gas/heavy-gas comparisons in simulation and analysis of the LAPPD sensor array. We also present results on MaPMT with MAROC sum readout bench test. Those results are presented in the sections below.

3.1.2 Project Summary

This report describes the completion of the four proposed milestones of the prototype gas Cherenkov pre-R&D project:

- The construction and delivery of a prototype gas Cherenkov was completed in early 2020. This prototype was designed and constructed at Temple University with a photosensor array of the same size and dimension as a single array for the SoLID heavy gas Cherenkov (a 4x4 MaPMT array) and total radiator gas length comparable to the length designed for both the SoLID light gas (LGC) and heavy gas (HGC) Cherenkov detectors. Each of the 16 MaPMTs in the 4x4 array was subdivided into 4 quadrants via an electronic summing board which was developed by the Jefferson Lab detector group.
- Cosmic rays testing and calibration of the detector, along with its ancillary detectors, was completed before installation into Jefferson Lab’s Hall-C. This included construction of a DAQ for the prototype test, as well as a baseline testing of each detector component.
- Both low and high rate data were successfully collected, from two different angular configurations, parasitically and within a truncated timeline due to pandemic-related restrictions at the facility. Low rate data for the MaPMT array was collected before the pandemic related lab shutdown in spring of 2020, where the detector was set-up at an angle of 75° and 17 feet from the Hall-C target. Parasitic data was taken to baseline the electronics at a rate of 320 kHz per PMT. After the lab resumed operations, the prototype was moved to the high rate location, 3.5° and 39 feet from the target, where a total rate of 4.8 MHz per PMT was recorded. This rate matched simulated expectations of high rate on the HGC PMTs. In both the low and high rate configurations, clean signals could be identified and overall electronics performance was near identical.

- High rate collection of data with MAROC sum electronics and subsequent analysis of the pixel and sum data was completed separately by the Duke group on the bench, primarily due to a truncated amount of parasitic running time available in the hall during the pandemic. The bench tests were able to simulate high rate signal and background using LED light, and test the linearity and response of individual pixel output through using MAROC electronics boards.

Along with these milestones, the overall goals and objectives of the Cherenkov project were also completed: The primary goal of the pre-R&D was to validate the response of the photosensor electronics array, a four-by-four grid arrangement of Hamamatsu 64-pixel multi-anode PMTs along with pixel summing electronics, under a high rate environment similar to or exceeding that expected during SoLID production running. We collected and analyzed both high and low rate (benchmark) data. From this we were able to:

- confirm that the electronics components were able to perform efficiently at higher rates than expected with SoLID running.
- conclude that, while a PMT summed approach could form an efficient trigger for the light gas Cherenkov (LGC) at high rates, a segmentation at the quadrant level per MaPMT would improve efficiency for electron identification.
- connect and tune the expected response of the electronics in geant4 (GEMC) simulation to the actual response seen at both low and high rate in the lab.

The secondary goals of the pre-R&D were also completed:

- Incom LAPPD (or large-area micro-channel plate PMT) as an alternative to the MaPMT was tested under the same conditions at low rate. The LAPPD in unison with the quadrant based segmentation electronics showed similar effectiveness and efficiency as that of the MaPMTs. In the study of the LAPPD, an exact SPE was not directly measured, which increases the uncertainty on the photo-electron count. This is not a limitation of the technology, but a result of our procedure. Even with this uncertainty, the results from our analysis show the LAPPD as a capable substitute for the MaPMT under similar conditions.
- The use of MAROC sum electronics allows pixel, quad and total sum analysis of the MaPMT response at the same time. The electronics were designed, produced and tested with cosmic rays at low rate and LED at high rate. Basic photoelectron and ring analysis were performed. Its sum signals shows similar efficiency to the simple summing electronics used during the beam test and the pixel signals are helpful for background rejection.

- Various unique components of the Cherenkov that are planned for the final design of both the LGC and HGC were also utilized in this test.
 - A mirror was constructed from reflectively coated Lexan film attached to a flat carbon-fiber blank. A sample of the reflective film was tested and confirmed to have the expected reflectivity at lower wavelengths, but the reflectivity of the mirror post-construction could not be measured directly due to the size of the mirror and available equipment.
 - The heavy gas (C_4F_8) proposed for use in the HGC was also used for some data collection in the pre-R&D parasitic set-up. The expected increase in cone-size and photoelectron count from simulation was also confirmed in the collected data.

3.2 Project Milestones

Milestone	Objectives	Expected Completion Date	Status
1	Construction and delivery of Cherenkov tank to Jefferson Lab.	Early January 2020	Complete (Q1)
2	Cosmic testing and installation into experimental hall.	Mid February 2020	Complete (Q1)
3	Collection and analysis of low and high rate data with electronic summing-board.	End of Year 2020 (+2 Month Contingency)	Collection complete (Q2), Analysis completed (Q4).
4	Collection and analysis of high rate data with MAROC electronics.	End of Year 2020 (+4 Month Contingency)	Completed on bench (Q6)

3.3 Budget and expense summary

To date funds have been used to purchase all the materials to construct the Cherenkov prototype tank with pressure controls, all connectors and cables for reading out signals of 64 channels from MaPMTs or LAPPD, mirror, MaPMTs, wavelength shifter coating, radiator gas, MAROC readout boards and their cabling. Funds have been used for the mechanical engineering design and machining as well as electrical engineering support, travel and transport of the prototype from Duke and Temple to Jefferson Lab, and the research personnel support for the approved activities at Duke, Temple and Argonne.

Category	Budget	Q1	Q2	Q3	Q4	Q5	Q6	Total
Material	\$210,000	\$124,736	\$84,414	\$3,311	(\$228.64)	\$0	\$ 4,021	216,253
Personnel	\$240,000	\$31,376	\$27,411	\$38,725	\$47,915	\$41,844	\$26,718	213,989
Travel	0	0	0	\$5,295	\$3,509	\$5,460	\$3,125	17389
Total	\$450,000	\$156,112	\$111,825	\$47,331	\$51,195	\$47,304	\$33,864	447,631

Table 3: Budget and expenditures summary from both Temple, Duke and Argonne for the Cherenkov prototype (overhead included).

3.4 Analysis and Simulation

This quarter, we have compared the Cherenkov signals from light gas and heavy gas. The beam test data were collected with the Incom LAPPD at large angle.

As shown in the previous report, with the light gas radiator (CO_2), a typical Cherenkov photon ring would have 9 to 10 fired quadrant channels. In heavy gas (C_4F_8), the Cherenkov light cone contains more photons and has a larger opening angle, resulting in a greater radius on the detection plane and more fired quadrant channels. According to their refractive index ($n_{\text{CO}_2} = 1.0005$ and $n_{\text{C}_4\text{F}_8} = 1.0014$), the Cherenkov ring from C_4F_8 is about 70% larger in radius than the ring from CO_2 . Thus, the corresponding coverage of a typical Cherenkov signal is 15 to 16 quadrant channels in the heavy gas. Figure 11 shows the Cherenkov rings we observed with the LAPPD and different gas radiators from the beam test at large angle. And the Geant4 simulation shows similar results in Figure 12.

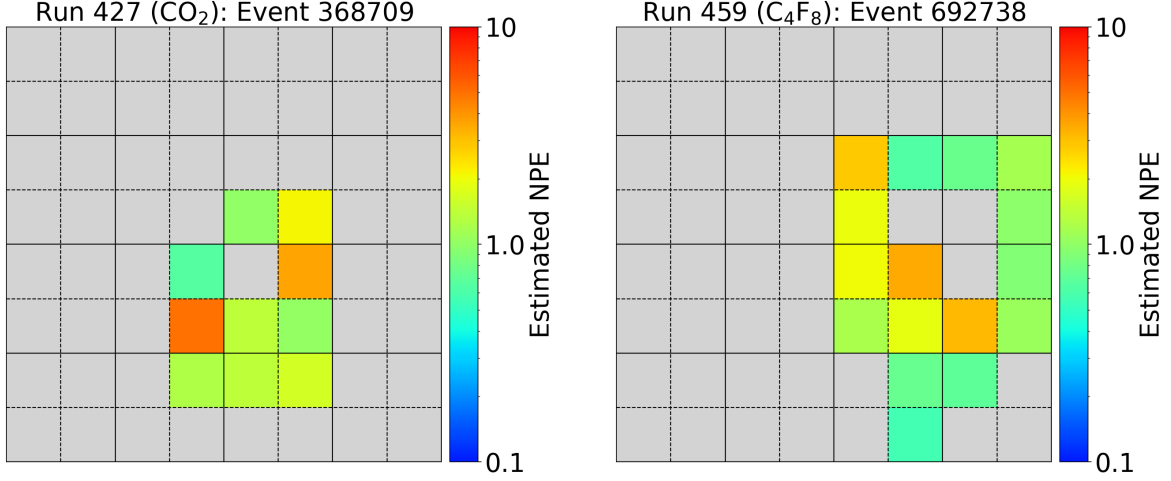


Figure 11: Event samples from LAPPD beam test data. Left: A Cherenkov photon ring from CO₂ that lights up 10 quadrant channels. Right: A Cherenkov photon ring from C₄F₈ that lights up 16 quadrant channels. The comparison shows that heavy gas (C₄F₈) produces larger Cherenkov photon rings.

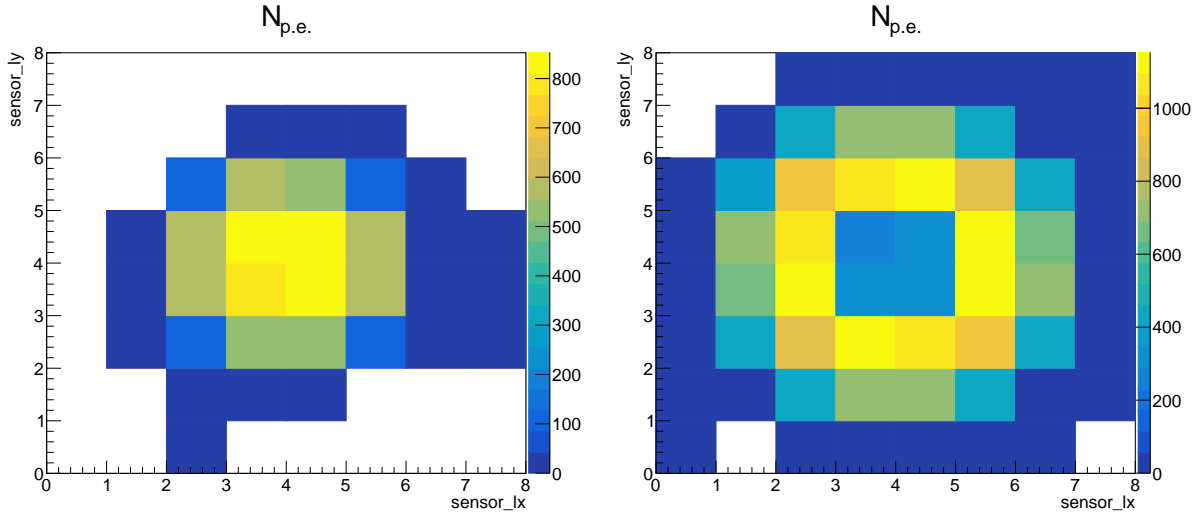


Figure 12: Simulation event distribution for the LAPPD beam test at large angle with electrons entering the center of the detector for CO₂ (left) and C₄F₈ (right). The rings sizes are similar to those observed in the test data.

Given the number of quadrant channels for typical Cherenkov events in different gas radiators, we sum all the signals with the requirement of 9 to 10 fired quadrants in CO₂ and 15 to 16 fired quadrants in C₄F₈. The signal sums with the LAPPD sensor show an NPE = 12 in CO₂ and NPE = 21 in C₄F₈. Our simulation can also well describe the difference

between the two gas radiators. The simulation yields $NPE = 9$ in CO_2 and $NPE = 23$ in C_4F_8 , showing a good agreement with the data.

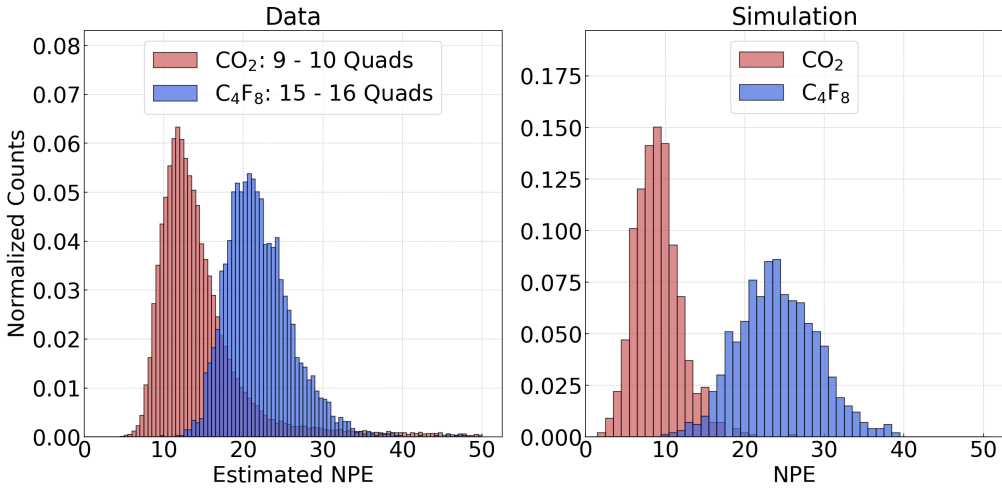


Figure 13: Comparison between Cherenkov signals from CO_2 and C_4F_8 . Left: Data taken with the LAPPD at large angle. Events with 9 or 10 fired quadrants are selected for CO_2 data, and with 15 or 16 fired quadrants for C_4F_8 data. The number of fired quadrants are chosen in accordance with the nominal coverage of the Cherenkov photon rings. Right: Simulation for the LAPPD response at large angle with electrons entering the center of the detector.

3.5 MaPMT with MAROC sum readout bench test

3.5.1 Sum saturation study

In addition to the TDC information from pixels of MaPMT, the MAROC sum electronics provides an analog sum of charge collected in a group of pixels. MAROC sum board sums the charge collected in a group of 8 pixels to provide a total of 8 analog sums as shown in Figure 14. For a quadrant signal, two sums each of 8 pixels are added and for the total sum, all 8 sums are added. For instance, quadrant 1 is the sum of “SUM1” and “SUM2”. The performance of MAROC electronics was validated by the CLAS12 RICH detector at lower rates, two orders of magnitude smaller than expected in SoLID. However, the MAROC sum board has not been used and tested yet. The output analog sum should be linear to the amount of charge injected. But if the injected charge is large enough then the MAROC sum starts saturating i.e the output signal won’t be linear to injected charge. We carried out a study to determine the maximum number of photoelectrons that a single pixel, quadrant, and sum signal can hold before saturation. Gain of the MAROC board can be set between 1 to 4. The gain of 1 means no amplification for the signal while the gain of 4 means the

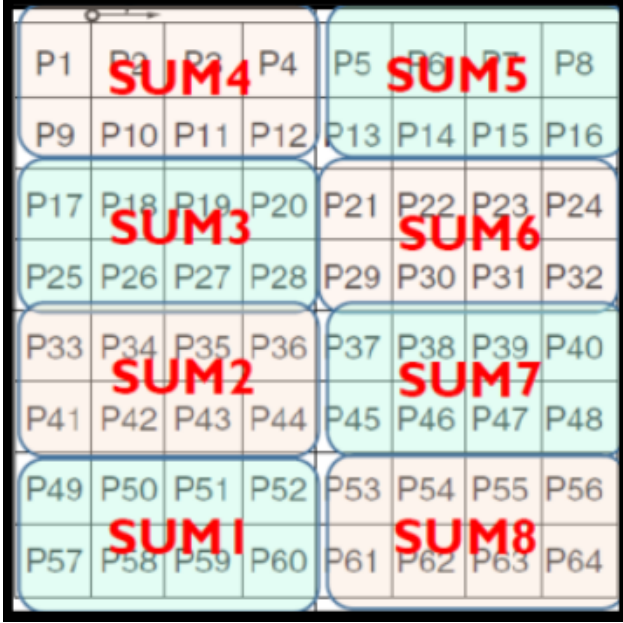


Figure 14: Schematic representation of summing mechanism of MAROC sum board for H12700 MaPMT series with 64 pixels. MAROC sum board sums group of 8 pixels. The “SUM1” and “SUM2”) give first quadrant signal, “SUM3” and “SUM4” give the second quadrant, and so on. The total sum is from the sum of all 64 pixels coming from 8 sums.

signal is amplified by a factor of 4. For our test, we injected the known charge in a step for a given pixel or group of pixels with the gain set to 1.

Figure 15 shows the number of photoelectrons (corresponding to MaPMT at 850 V) for different injected charges with only one pixel fired. The red line is a linear fit to the data. The blue vertical and horizontal dashed lines represent the threshold charge in DAC and number of photoelectrons respectively above which the sum signal saturates. Using the measured value of the position of the mean peak of a Single Photoelectron (SPE) distribution the ADC value is converted to a number of photoelectrons (NPE) that a pixel can withstand before saturation. The saturation limit varies with the number of pixels fired in a group of 8 pixels shown in Figure 14. Table 4 shows the maximum number of photoelectrons for an individual pixel, quadrant, and total sum below which the MAROC sum is linear to the injected charge at different High Voltage (HV) settings for a MaPMT. The linear range decrease with increase in HV applied to MaPMT.

3.5.2 Pixel TDC threshold study

For MAROC pixel readout, MaPMTs in the detectors like CLAS12 RICH are usually operated at around 1000 V. As discussed in section 3.5.1, we could get benefit from the larger dynamic range if we could operate MaPMT at lower HV. To find the optimized value of

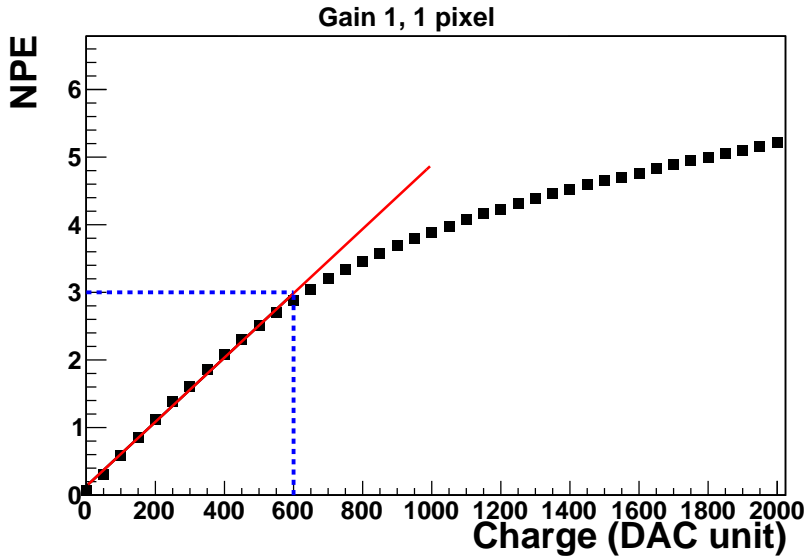


Figure 15: Saturation study of MAROC sum board with one pixel fired and MAROC pre-amplifier gain set to 1. The number of photoelectrons vs injected charge in DAC unit. The red line is a linear fit to the data. The maximum value of charge injected and the number of photoelectrons before saturation is shown by the dashed blue vertical and horizontal lines for MaPMT at 850 V.

the TDC threshold at 850 V we plotted the duration of a hit at different TDC thresholds. The duration of a hit is defined as the difference in time when the trailing and leading edge crosses the set TDC threshold. The duration of a hit depends on the amplitude of a signal. For cross-talk (small amplitude) the duration of a hit is small compared to the signal. Figure 16 shows the duration of hit distribution for 3 typical TDC discriminator threshold values 10, 30, and 50 DAC units above the average pedestal value. At the lower threshold, we record a lot of lower amplitude cross-talk and at the higher threshold, we may miss a large part of the single photoelectron distribution. After these tests, the common discriminator thresholds were set to +30 DAC units above the average MaPMT pedestal position, a level that corresponds to a small fraction of the average SPE amplitude. To make sure that our choice of TDC threshold does not reject the SPE signal we compared the number of photoelectrons distributions for two identical runs with the same TDC threshold, +30 above the mean pedestal. The red and blue distribution in Figure 17 corresponds to MaPMT at 1000 V and 850 V respectively. The mean of the NPE distribution of 850 V is about 95% of the distribution of 1000 V and it suggests that MaPMT at 850 V, TDC threshold of +30 DAC units above pedestal mean is still sufficient to record the small-amplitude signal.

	Number of pixels fired		
HV (V)	1 pixel	16 pixels (Quad)	64 pixels (Total Sum)
850	3	10	44
900	2	7	29
1000	1	4	17

Table 4: Saturation limit for the MAROC sum board in terms of NPE for a single pixel, Quad, and total sum signal at different high voltage for MaPMT. For this study, MAROC pre-amplifier gain is set to 1. With the increment in HV applied to MaPMT the linear dynamic range gets reduced.

3.5.3 LED Ring analysis

In the Cherenkov detector, the Cherenkov ring is analyzed for particle identification. To study the performance of MAROC sum electronics and the efficiency of our algorithms we analyzed the ring formed at MaPMT in presence of background comparable to SoLID running condition. We analyzed both pixel and sum data using two algorithms to identify the signal in presence of background which is produced by another LED.

- Number of photoelectron cuts which is most straightforward
- Hough circular transform, the ring finder algorithm from computer vision

The accuracy or Figure of Merit (FOM) is defined as in Equation 1 for signal events and Equation 2 for background events to test the performance of the algorithms. The ideal result would have both FOM as large as possible and at least larger than 90%.

$$Accuracy/FOM = \frac{\text{number of accepted signal events}}{\text{total signal events}} \quad (1)$$

$$Accuracy/FOM = \frac{\text{number of rejected background events}}{\text{total background events}} \quad (2)$$

Two similar LEDs (275 nm) were enclosed inside a box. The pulsed light from the first LED was passed through the circular filter to form a ring near the center of the MaPMT array with a radius close to 8 pixels. The second LED was operated with DC voltage to provide continuous background. The background level from the second LED was controlled by adjusting the voltage of its DC power supply. Figure 18 shows the schematic experimental setup to produce the LED rings. We collected the data at a different level of background up to almost twice as expected in the SoLID running condition. Position and ring size are

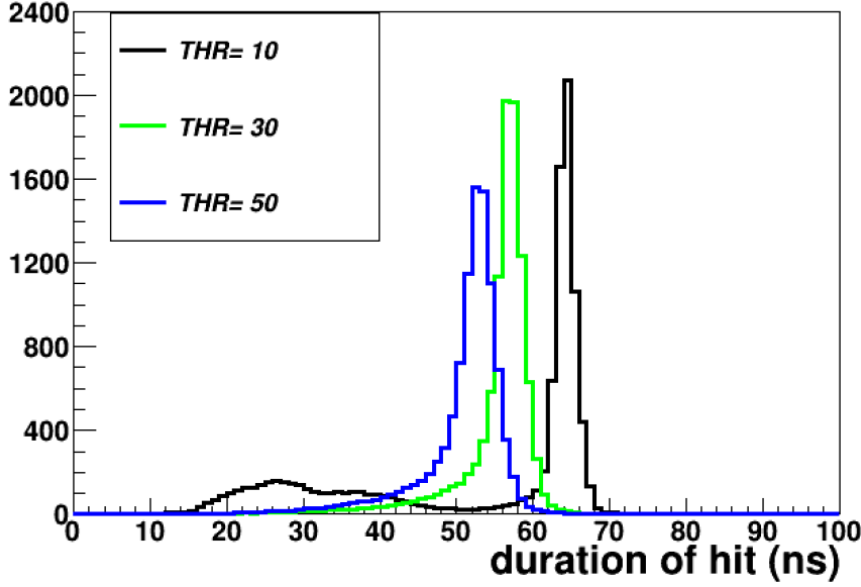


Figure 16: Duration of hit distribution from pixel readout of the MAROC sum board at 3 different values of thresholds 10, 30, and 50 DAC units above the average pedestal position, with MAPMT at 850 V.

fixed for the LED ring so they are relatively simple to identify from the background. But still helps us to test the performance of our algorithm.

Figure 19 shows at the lower background level, less than 200 kHz/pixel, the background distribution is well separated from the signal in presence of background. At these lower background rates, the simple number of photoelectron cuts is sufficient enough to separate the signal from a background with better than 90% accuracy. But at a higher background rate, the background and signal (in presence of background) distribution are more overlapped and the number of photoelectron cuts is not sufficient enough to reject the background from the signal. At higher background the more complicated Hough transform algorithm is used. With Hough transformation, the accuracy is improved from 70% to 92% at the random background of 370 kHz/pixel. The parameters of the recognized rings were reconstructed using Hough transformation. Figure 20 shows the reconstructed parameters of ring radius, X, and Y positions of the LED ring at various background rates. The reconstructed parameters are in good agreement with the experimental setup.

We also analyzed the sum readout results for the same LED ring data. The quad sum readout using Hough transformation method can provide similar separation with larger uncertainty than the pixel readout. It's much more difficult for total sum readout to use Hough transformation method because the ring only covers about 4 PMTs.

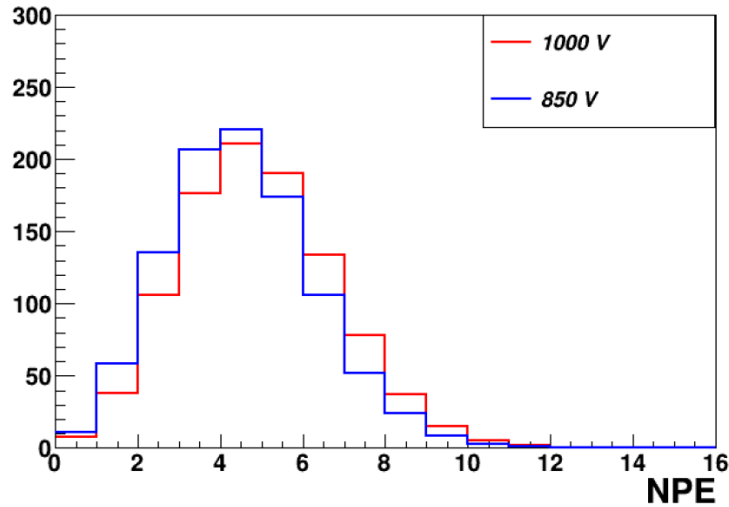


Figure 17: A number of photoelectrons (NPE) distribution with TDC threshold +30 DAC unit above pedestal for two identical settings. The NPE distribution with MaPMT at 1000V is represented by the red histogram while the blue histogram is for MaPMT at 850 V.

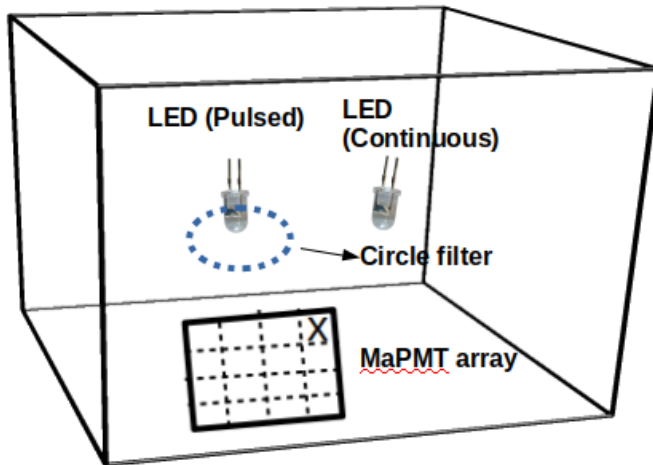


Figure 18: Schematic layout for LED ring. For signal, we used pulsed LED. Light from the pulsed LED is passed through the circular filter before it is collected in the MaPMTs array, 15 MaPMTs shown by the grid. The second LED operated with DC voltage provides the background. The entire setup was placed inside the black box to avoid any external light.

3.5.4 Cosmic test

We also tested the Cherenkov ring produced using the cosmic muon. Figure 21 shows the schematic layout for the cosmic ring test. As the cosmic muon passes through the 4 cm lucite radiator, refractive index of 1.5, the Cherenkov light is emitted then collected in 15 MaPMTs array. The opening angle of Cherenkov light (48.2°) is larger than the critical angle of lucite for total internal reflection (41.8°). As a consequence, the Cherenkov light

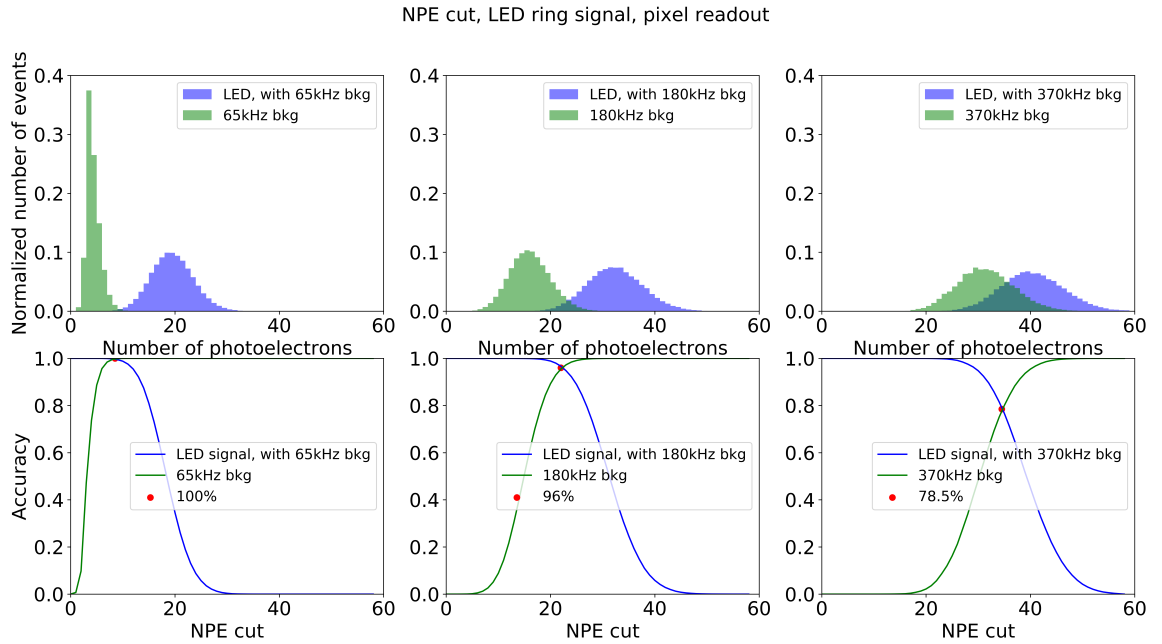


Figure 19: Top: Number of photoelectron distribution for LED ring with pixel readout. The green and the purple histogram represents a number of photoelectrons with background only and LED signal in presence of background. The histograms are at the background rate of 65, 180, and 370 kHz/pixel from left to right. Bottom: The figure of merit for the number of photoelectrons cut at different levels of background.

emitted with vertical cosmic muon won't be able to pass through the lucite surface to reach to the MaPMT array. To take the advantage of vertical muon flux we tilted the lucite by 12° . After tilting the lucite we were able to collect the Cherenkov light produced by the muon with an incident angle between 0 to 6° (angular acceptance of muon between the green and vertical black lines) while muon striking from another half (between the black and red lines) were missed due to the total internal reflection and acceptance of the MaPMT array. The trigger was formed by two scintillators S1 and S2, about 5 cm x 5 cm overlapping area, in coincidence. The muon can hit anywhere within the 4 central MaPMTs shown by the red rectangle and form a cluster at the MaPMT array. The expected position of partial (about 35%) Cherenkov ring and muon cluster is shown in Figure 21 (right).

Compared to the setting reported in quarter 5, we changed the position of lucite and the scintillators so that a larger portion of the ring (about 35%) can be observed on MaPMT. By moving scintillators and lucite the data collection rate was decreased but the average number of photoelectrons increased to 32. Figure 22 (left) shows the number of photoelectrons in the Cherenkov ring with and without different levels of background from the LED. The right plot shows the number of photoelectrons within the signal time window at different background

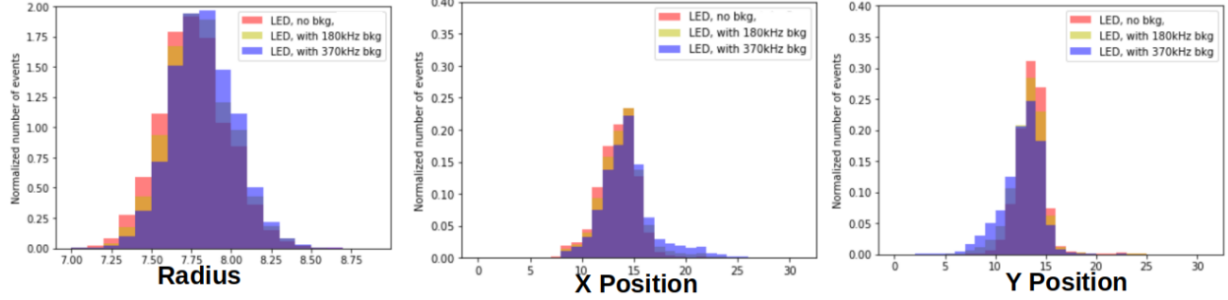


Figure 20: Parameters of the recognized rings using the Hough transformation for pixel readout. The reconstructed radius and position of the ring are in agreement with the experimental setup.

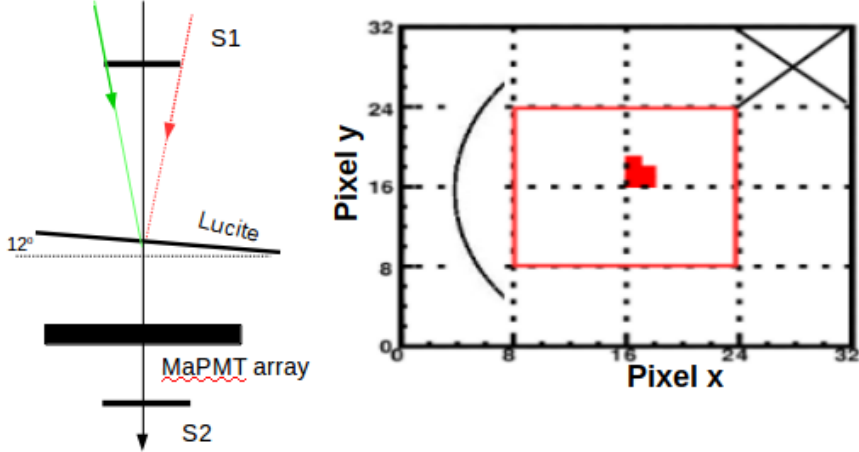


Figure 21: Left: Schematic layout for the cosmic test. Two scintillators, one at the top and another at bottom of the PMT array form a trigger. Lucite is tilted at an angle 12° with horizontal. The red and the green lines represent the extreme of scintillator acceptance. Due to the total internal reflection and the limited size of the MaPMT array, only about half of the triggered events form the partial ring. Right: The 15 PMTs array of dimension $\sim 20 \times 20$ cm is used to detect the Cherenkov ring. The cosmic muon can hit any of the central 4 PMTs represented by the red rectangular box.

levels 117, 190, and 320 kHz/pixel. The observed number of photoelectrons is close to what we expect. Because the lucite is 4 cm thick and there is no optical focusing, a very broad ring with its width close to 4 cm is formed for each event. And as the muon hit position varies within a couple of MaPMTs, the ring position also changes accordingly event by event. Those conditions make the ring distribution complicated and the Hough transformation is not the right tool for analysis any more. Machine learning algorithms may be useful for the more complicated ring analysis and we plan to explore it first with the SoLID Cherenkov

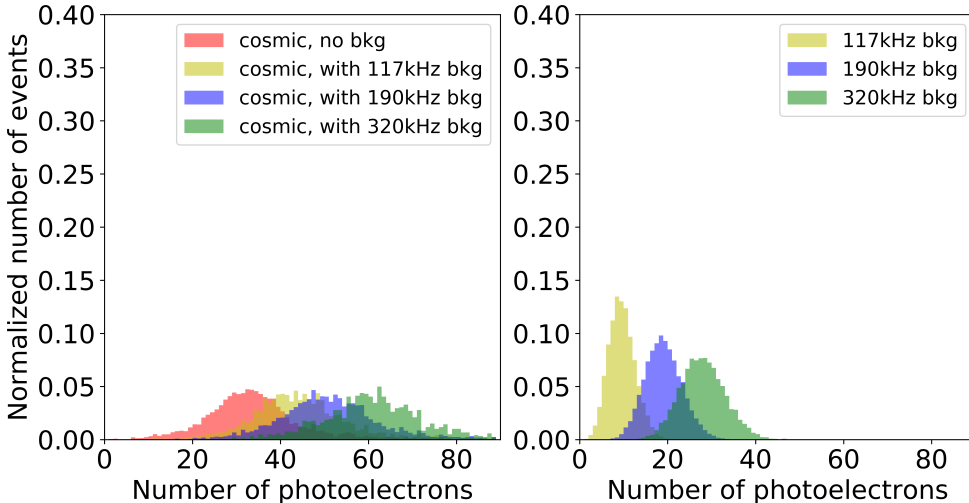


Figure 22: The number of photoelectrons within the signal time window of pixel readout. Left: Number of photoelectrons with and without different levels of background. Right: The number of photoelectrons with the background at 117, 190, and 320 kHz/pixel. The observed number of photoelectrons for a cosmic event and background event at different levels match the expected number.

detector simulation, but that is beyond the scope of the pre-R&D.

3.6 Discrepancies between measured and simulated NPE count and possible sources of NPE inefficiency

The average number of photoelectrons (NPE) detected for the MaPMTs array analysis in this study remained close to 50-60% of the predicted NPE from the Geant4 simulation for all configurations. While this NPE number was more than enough to perform the required analysis for the pre-R&D goals, it does leave the question to what caused the loss of collected photons. The most likely places where NPEs can be reduced are: impurities in the radiating gas, reduced efficiency of the PMT, reduced gain on the wave-length shifting PMT coating, misalignment of optics, and reduced reflectivity on mirror surfaces. The gas filling procedure was standard practice pumping of 99+% pure CO₂, and the pressure regulator operation was cross-checked against analog pressure gauges on the device making gas impurity an unlikely source. The MaPMTs (and LAPPD) were p-terphenyl coated according to guidelines that have repeatedly shown consistent gains on NPEs, which also leaves the WLS coating an unlikely source of the NPE loss. The reduction of NPEs was consistent across all MaPMTs on the detector array, making individual variations in quantum-efficiency or an optical misalignment also unlikely. The loss of NPEs most likely can be attributed to the

reflectively of the primary mirror used in this study.

The telescopic Cherenkov device used a flat elliptical mirror that was constructed from a thin carbon-fiber back-plate to which a reflectively coated film of Lexan polycarbonate was applied. The lexan was cut to the required elliptical shape and coated at Evaporated Coatings Incorporated (ECI), and delivered to Temple University with small-size square samples that were coated at the same time in the same batch as the larger ellipse. These samples were then tested and shown to have the expected reflectively ($\geq 80\%$) at lower (250 nm) wavelength. The primary elliptical film was never directly tested. There are some possible sources where reflectively of the elliptical mirror could have been impacted. The ellipse was sent to Temple with a removable protective film to avoid damage in transit. The type of protective film used to cover the samples was different than the type used to cover the ellipse, due to the larger size of the ellipse. Removal of the protective film must be done carefully as not to damage the reflective coating, and the difficulty of removing the protective film scales with the size of the mirror. After removal of the film there were obvious optical defects on the surface of the mirror (small localized wrinkles) that were likely present before the removal of the protective film. The reflective film was glued to the polished carbon-fiber blank using an aerosol adhesive. This was done carefully, but not in a clean room environment. Then felt cloth was draped over the reflective surface and additional weight was put on top of the felt to secure the film to the carbon-fiber while the glue dried. Finally, the mirror was carefully transported with the tank to Jefferson Lab where it was assembled and aligned.

Any of the above listed items or steps may have impacted the reflectively of the mirror. A systematic testing of each step in the above procedure would have been required to determine where reflectively may have been lost, but such studies were outside the scope of the proposed pre-R&D. The final reflectively of the mirror may be determined by cutting (destroying) the elliptical mirror to obtain a sample small enough to measure, but the TCD, including it's mirror, is currently being used for additional R&D at Jefferson Lab. A separate pre-R&D proposal to test mirror design using a similar procedure would also systematically test each stage of mirror fabrication to discern where reflectively may be lost and to what amount. Such a pre-R&D proposal has been submitted to DOE through the New Mexico State University Nuclear Physics Group.